PHILOSOPHICAL MAGAZINE, 2003, VOL. 83, NO. 12, 1407–1419

Grain boundary structure of nanocrystalline Cu processed by cryomilling

J. Y. HUANG†, X. Z. LIAO, Y. T. ZHU

Materials Science and Technology Division, Los Alamos National Laboratory
Los Alamos, New Mexico 87545, USA

F. ZHOU

Department of Chemical and Biochemical Engineering and Materials Science,
University of California, Irvine, California 926971, USA

and E. J. LAVERNIA

Department of Chemical Engineering and Materials Science, University of
California, Davis, California, USA

[*Received 18 January 2002 and accepted 31 December 2002*]

ABSTRACT

The microstructures of cryogenically ball-milled Cu were investigated by high-resolution electron microscopy. It was found that the grain-size reduction is a dislocation-controlled continuous process which consists of the formation of small-angle grain boundaries (GBs), a gradual increase in misorientations as a result of accumulation of more dislocations and, finally, the formation of large-angle GBs. The GBs were generally curved, wavy or faceted, and heavily strained, which are typical characteristics of nanostructured materials. In addition, extrinsic dislocations were found in many GBs, indicating that most are in a high-energy non-equilibrium configuration, which is consistent with observations in equal-channel angular pressing processed Cu, Ni, and Al–Mg, repetitive corrugation and straightening processed Cu and room-temperature ball-milled Cu. These results support a still-disputed concept that GBs in nanostructured metals processed by severe plastic deformation are mostly in non-equilibrium states.

§1. INTRODUCTION

Ball milling has been proven to be a versatile technique for production of large quantities of nanocrystalline powders which can be sufficient for industrial application. It is a typical 'top-down' approach during which coarse-grained materials are decomposed into nanocrystalline building blocks under severe plastic deformation. Although this technique has been extensively used in both research laboratories and industries to synthesize nanostructured materials, detailed microstructural evolution during this process remains unclear, which severely hinders understanding and further application of this technique. The grain sizes of the ball-milled powders are usually less than 100 nm. Thus, conventional transmission electron microscopy inves-

† Current address: Department of Physics, Boston College, Chestnut Hill, Massachusetts 02467, USA. Email: huangje@bc.edu.

Philosophical Magazine ISSN 1478–6435 print/ISSN 1478–6443 online © 2003 Taylor & Francis Ltd
http://www.tandf.co.uk/journals
DOI: 10.1080/1478643031000083633

tigation cannot provide much information regarding dislocation configurations or grain boundary (GB) structures. In this context, high-resolution electron microscopy (HREM), which can provide atomic-scale structural information, is stringent. So far only limited effort has been given to the atomic structural investigation of ball-milled materials (Huang *et al*. 1994a,b, 1996, 1997a,b, 1998a,b, Shen *et al*. 1995, Huang 1999, Yang *et al*. 1999, 2000). This is possibly because ball-milled powders are usually agglomerated to large dense particles of micron scale, which makes it very difficult to obtain a thin region of a few nanometres or a tenth of a nanometre that is suitable for HREM. This makes it impractical to observe the ball-milled powders directly. Nevertheless, two techniques have been developed to obtain high-quality HREM samples (Huang *et al*. 1994a,b). These techniques have proved to be versatile ways to obtain directly atomic-scale structural information of the milled powders. Another practical way to obtain high-quality samples suitable for HREM is the following: the milled powder was cold compacted to a pellet and then ion milling or jet polishing was applied. This technique is suitable for ductile metals, such as Cu, Al and Zn.

Applying the above techniques, numerous deformation structures produced by ball milling have been revealed. For example, we observed room-temperature deformation twins in ball-milled Cu (Huang *et al*. 1996), which is unusual since Cu has enough slip systems (12) to accommodate the deformation at room temperature. We also observed nanograins deforming by simultaneous shearing rather than by the normal dislocation slip under high strain rates induced by ball milling (Huang *et al*. 1998a). These results provide not only deep insight into the ball-milling process but also new understanding of nanostructured materials.

The GB structure of nanostructured metals processed by severe plastic deformation is suggested to be in a non-equilibrium state (Horita *et al*. 1996, 1998, Huang *et al*. 2001, Valiev *et al*. 2000). The non-equilibrium GBs were proposed to be characterized by the presence of high density of extrinsic defects, such as dislocations and vacancies (Valiev *et al*. 2000). However, direct evidence of non-equilibrium GBs was not present until recently (Huang *et al*. 2001). Huang *et al*. (2001) found that extrinsic dislocations that are not geometrically necessary indeed exist in the GBs of Cu processed by repetitive corrugation and straightening (RCS). It is interesting to investigate whether the GBs in ball-milled nanostructured materials are also in non-equilibrium states. It is also practically important to investigate the GB structure of different nanostructured materials, since the change of GB structure can result in the change of physical and mechanical properties.

We report in this paper atomic-scale GB structure of nanostructured Cu after cryogenic ball milling in liquid N_2. The GB structure is compared with those observed in other cold deformation techniques, such as equal-channel angular-pressing (ECAP) (Horita *et al*. 1996, 1998) and RCS (Huang *et al*. 2001).

§ 2. Experimental procedure

A commercial Cu powder (99.5% + pure) with a particle size of about 300 mesh was used for the milling experiments. The milling was carried out in a modified Union Process 01-HD attritor with a stainless steel vial and balls (6.4 mm in diameter) at a rate of 180 rev min^{-1} for 8 h. The ball-to-powder weight ratio was 40 to 1. During the milling operation, liquid N_2 was added into the mill to maintain complete immersion of the milling media, which keeps the temperature at $-196^{\circ}C$.

The as-milled powders were cold compacted to a disc of diameter 4.4 mm under a pressure of about 3 GPa. The disc was then mechanically polished to a thickness of

about 20 μm and then ion milled for about 1 h suitable for HREM observation. The HREM experiment was carried out in a JEOL 2010F electron microscope operated at 200 kV. The grain sizes were normally less than 100 nm so that tilting of individual grains was very difficult. Thus, HREM images were taken randomly in a number of grains.

§ 3. Results

3.1. *Grain size and general morphology*

The grain size of the cryomilled Cu was not homogenous, and it varied from region to region. The morphology of the grains also changed dramatically in

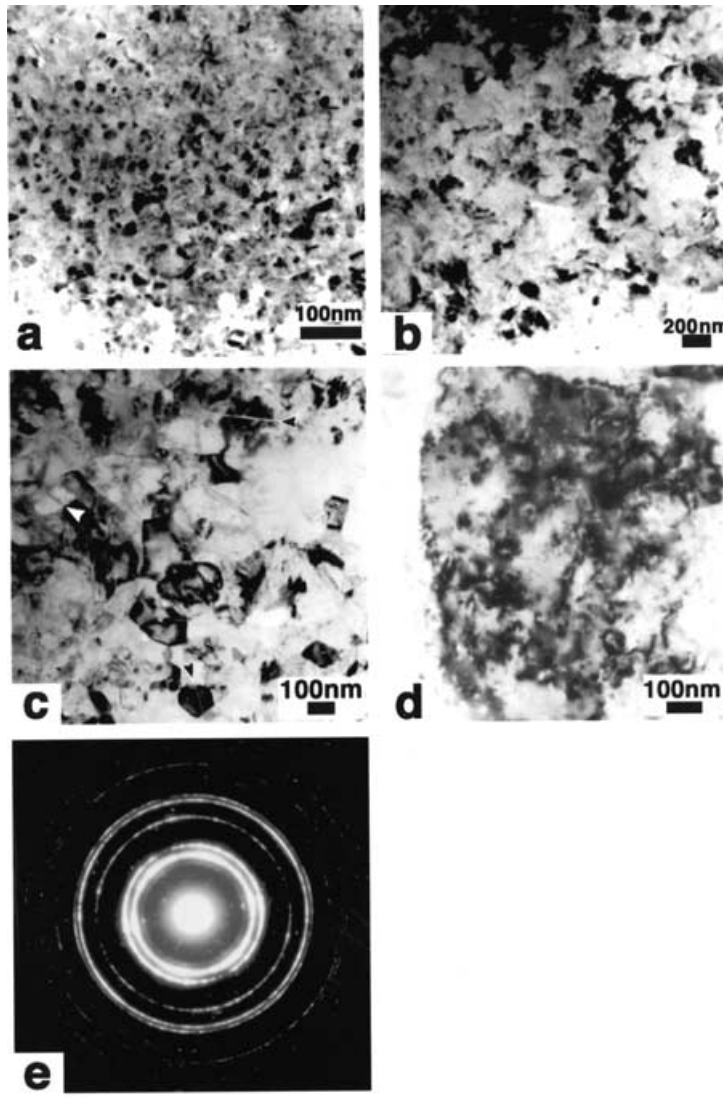

Figure 1. (*a*)–(*e*) A general morphology of cryomilled Cu with different grain sizes and morphologies. (*e*) A representative electron diffraction from the nanograins.

different regions. Typical transmission electron micrographs are shown in figures 1 (*a*)–(*d*). In figure 1 (*a*), the grain size is approximately 10–20 nm, which is the smallest grain size observed in this sample. The grain structures in figure 1 (*b*) are not well developed, and the GBs are not well delineated, possibly owing to the extremely irregular shape and overlapping of grains. The grain size in figure 1 (*b*) is about 70–80 nm, and this was the most frequently observed morphology in this sample. In contrast with figure 1 (*b*), individual grains are well defined in figure 1 (*c*), and most of the GBs are very sharp. The grain size in figure l (*c*) is larger than in figure 1 (*b*), and the largest size is about 160 nm. Defects in the interior of grains are readily visible, as indicated by the arrowheads. These defects are either stacking faults (SFs) or twins. In a rare case, very large grains were observed, and a typical example is shown in figure (*d*), which shows a grain of about 600 nm. The dislocation density in such a large grain is very high, and cell structure is also visible. These results indicate that deformation in the ball-milling process is not homogeneous. Figure l (*e*) is a representative electron diffraction pattern from the cryomilled Cu that shows diffraction rings typical for nanostructured materials. The diffraction rings show 111 and 200 texture.

3.2. *Defects in the grain interior*

Dislocations were found in most large grains with sizes greater than 50 nm. The dislocations identified by HREM were mostly of a 60° mobile type; these are typical dislocations in Cu after deformation (Huang *et al.* 1996, 2001). Besides dislocations, another important defect frequently observed in cryomilled Cu is deformation twins, an example of which is shown in figure 2. These multiple twins contain a giant step as indicated by the arrowheads in figure 2. The lattice in the step region is incoherent. Such a giant step can be associated with very complicated dislocation configurations. We were unable to identify these dislocations because the image was not clear enough to identify the core of the dislocations, and the step was possibly in a non-equilibrium state.

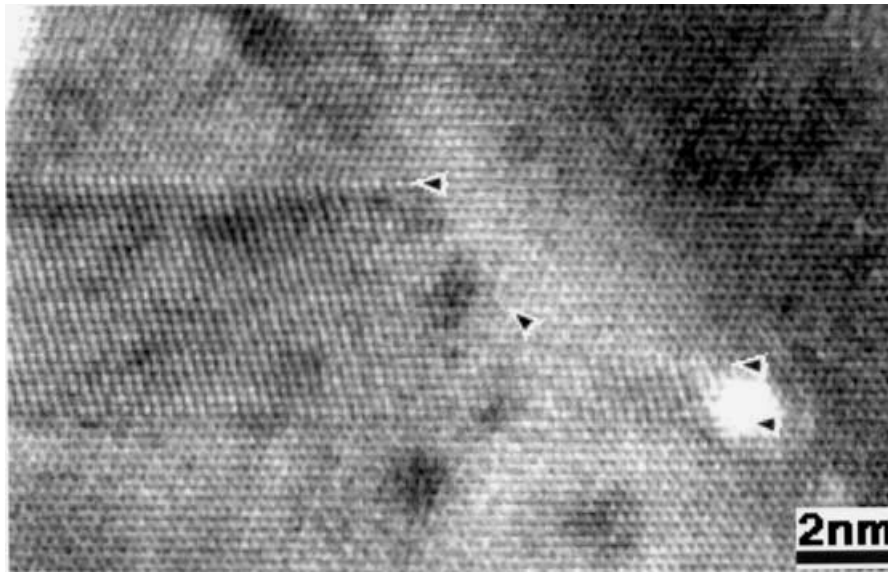

Figure 2. Deformation twins in cryomilled Cu. The arrowheads indicate a giant step.

When deformed at room temperature, slip rather than twinning is the preferred mode of deformation for Cu, because Cu has an intermediate SF energy, and twinning is difficult to occur at room temperature condition. However, as pointed out by Huang *et al*. (1996), under certain circumstances, such as a small grain size, high strain rate and low temperature, twinning can become the preferred mode of deformation. Deformation twins were found in ball-milled Cu even under room-temperature conditions. In the present case, the milling was performed at liquid-N_2 temperature so that deformation twinning occurs more readily.

3.3. *Grain boundary structure*

Figure 3 shows an asymmetric-tilt small-angle grain boundary (SAGB) and four dislocations that are almost periodically distributed. If one assumes that the electron beam is parallel to $\mathbf{B} = [1\bar{1}0]$, the Burgers vector of the dislocations is determined to

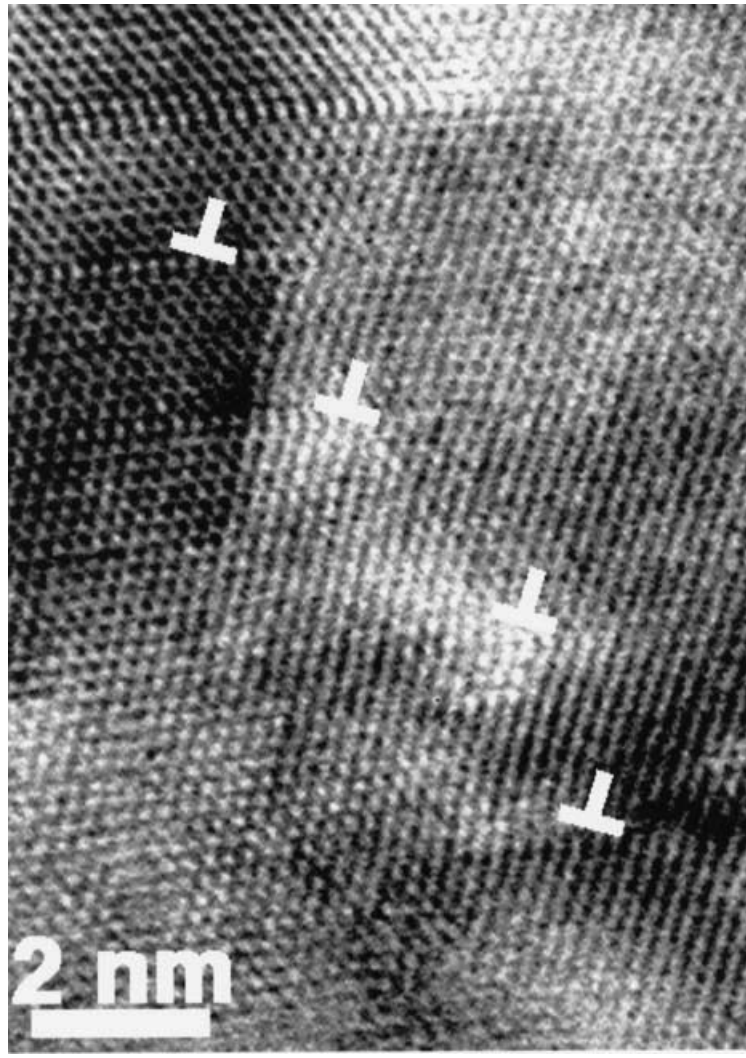

Figure 3. An asymmetrical SAGB. The white inverted Ts indicate the cores of the GB dislocations.

be $\mathbf{b} = \frac{1}{2}[10\bar{1}]$, which makes them 60° dislocations. Based on the simplified Frank formula, the spacing of the dislocations can be calculated to be $d = b/\theta$, where θ is the misorientation angle between the two grains and is about 6° in the present case. The calculated spacing between dislocations is 2.42 nm, which agrees very well with the experimental value of 2.45 nm. The SAGB is therefore well described by the simplified Frank formula. This SAGB does not contain extrinsic dislocations and is in equilibrium state.

Figure 4 is another asymmetrical tilt SAGB, and the misorientation angle is about 6°. The Burgers vector of the dislocations in the SAGB is again $\mathbf{b} = \frac{1}{2}[10\bar{1}]$. The interesting point in this SAGB is that there are two intersecting SFs on the two sets of {111} planes crossing the SAGB. As such, the SFs are bent after crossing the SAGB. This means that the SAGB cannot prevent the propagation of dislocations. The SFs are apparently generated by dissociation of two 60° dislocations, the cores of which are indicated by two inverted white-edged black Ts and $\mathbf{b}_1$ and $\mathbf{b}_2$.

We show how a SAGB is formed by the introduction of dislocations in figure 5. The GB is outlined by two types of strip (some of which are indicated by white arrowheads), which extend on the two sets of {111} planes. These strips are actually SFs or thin twins, which are associated with the dissociation of two 60° dislocations,

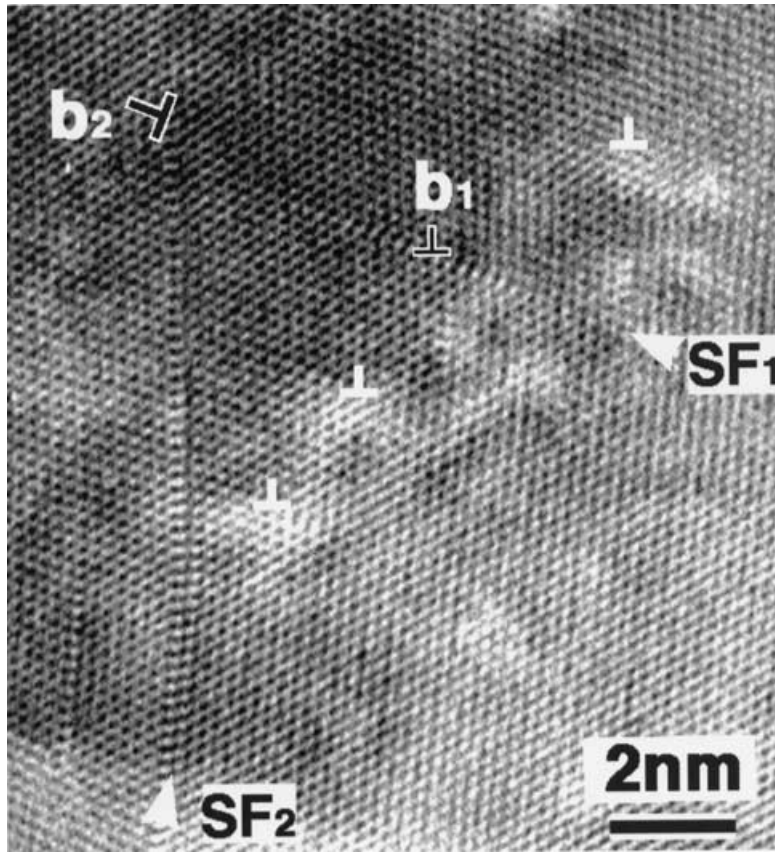

Figure 4. An asymmetrical SAGB. The white inverted Ts indicate the core of the GB dislocations. SF_1 and SF_2 are two intersecting SFs. The Burgers vectors $\mathbf{b}_1 = \frac{1}{2}[10\bar{1}]$ and $\mathbf{b}_2 = \frac{1}{2}[101]$.

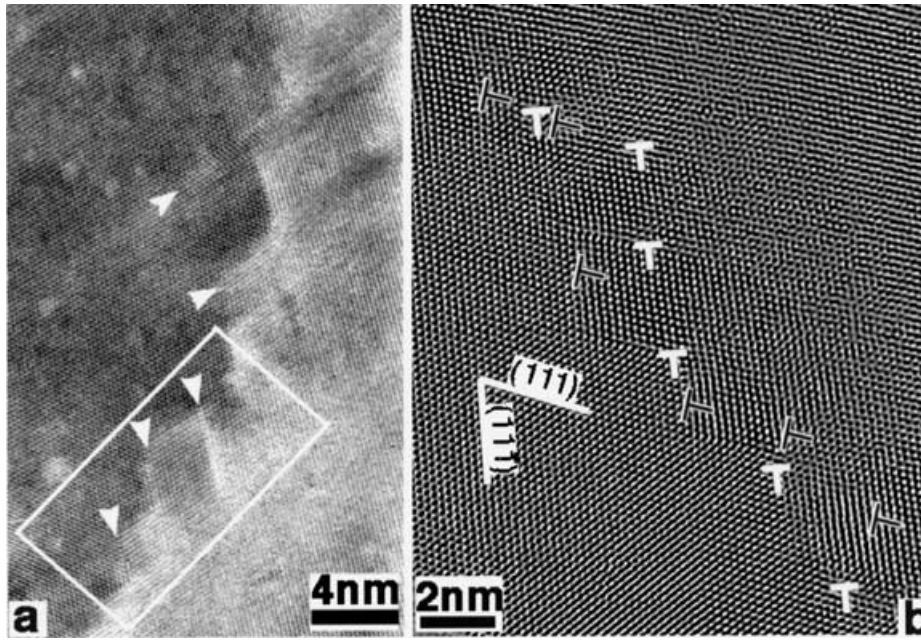

Figure 5. (*a*) An asymmetrical SAGB; the white arrowhead indicate SFs or twins in the two sets of {111} planes. (*b*) A local magnification of the region outlined in white in (*a*); the white Ts indicate the cores of the GB dislocations.

as indicated by Ts in figure 5 (*b*). These dislocations are slightly dissociated, thus producing the SFs and thin twins. The misorientation between the two grains is about 2° because of the introduction of these dislocations. A similar SAGB was also observed in ball-milled Cu (Huang *et al.* 1996) and in ECAP-processed Al–Mg (Horita *et al*. 1996).

Figure 6 shows a SAGB with a misorientation angle of approximately 16.5° reaching the limiting angle for that of a SAGB. The GB is curved and cannot be described by the simplified Frank formula. However, the Burgers vector of the GB dislocations is still a lattice vector, which is not the case for a large-angle grain boundary (LAGB). It is thus reasonable to classify such a GB as a SAGB. It is noted that for such a SAGB, the lattice is severely distorted in the GB region.

Figure 7 shows a SAGB with a misorientation of about 10°. The lattice spacing is approximately 1.8 Å which corresponds to that of Cu(200). The GB plane is curved. In order to locate cores of the mismatch dislocations, the original image in figure 7 (*a*) was Fourier filtered and shown in figure 7 (*b*), from which it is clearly seen that many mismatch dislocations were present in the GB region. According to the misorientation angle, the periodicity of the mismatch dislocations should be 66 lattice spacings. This means that geometrically necessary dislocations should appear in every 66 (200) lattice spacings. However, the actual observed dislocation periodicity is about 13 (200) lattice spacings, as seen in figure 7 (*b*). So many extrinsic dislocations which are not geometrically necessary were present in the GB. This infers that such a SAGB is a non-equilibrium GB.

Figure 6. An asymmetrical SAGB. The T and inverted Ts indicate the cores of the GB dislocations. The misorientation between the two grains is 16.5°.

Figure 8 shows GBs among three grains. The misorientation angles between grains 1 and 2, grains 2 and 3, and grains 3 and 1 are about 5°, 19° and 11° respectively. The GB between grains 1 and 2 is a SAGB produced by dislocations, while that between grains 2 and 3 appears to result from direct shearing, as evidenced by the narrow band present in the GB. The GB between grains 1 and 3 is curved and strained in several regions, and Moiré fringes due to overlapping of the two grains can also be seen.

Figure 9 is a near-symmetrical tilt SAGB. The dislocations are not aligned in one lattice plane yet, and dislocations with opposite Burgers vectors are shown close to each a other. Therefore, this segment of GB has a high energy and is in a non-equilibrium state.

Figure 10 is a near $\Sigma = 11$ LAGB. The GB plane is flat and slightly strained. Figure 11 shows a LAGB which exhibits a stepwise arrangement of facets parallel to (111) planes, and each facet consists of four to six layers of (111) planes. In figure 12 are shown a number of grains and GBs. In grains 1 and 2, deformation twins are seen. The deformation twins in grain 2 are initiated from the GB and terminated in the interior of the grain, meaning that the GB is heavily strained, thus becoming a nucleation site for other defects. The GB between grains 1 and 2 is a SAGB. The GBs are generally curved and strained and, in several regions, lattice disordering is observed.

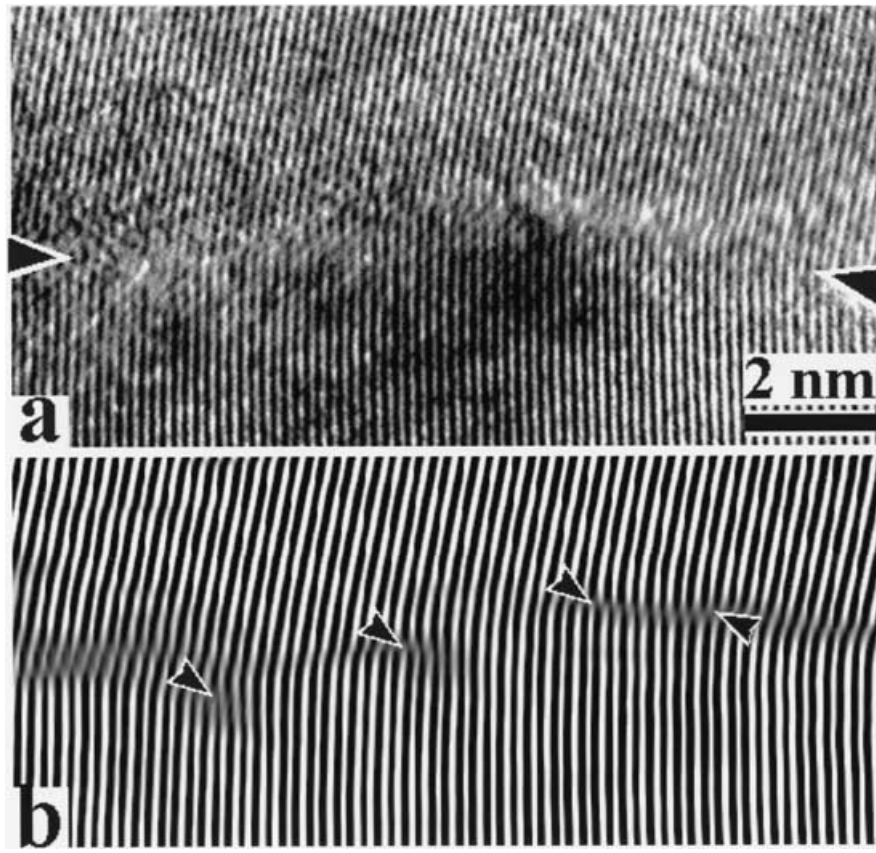

Figure 7. An asymmetrical SAGB. (*a*) The original image; the arrowheads denote the GB. Filtered image from a segment of (*a*); the arrowheads indicate the cores of the mismatch dislocations.

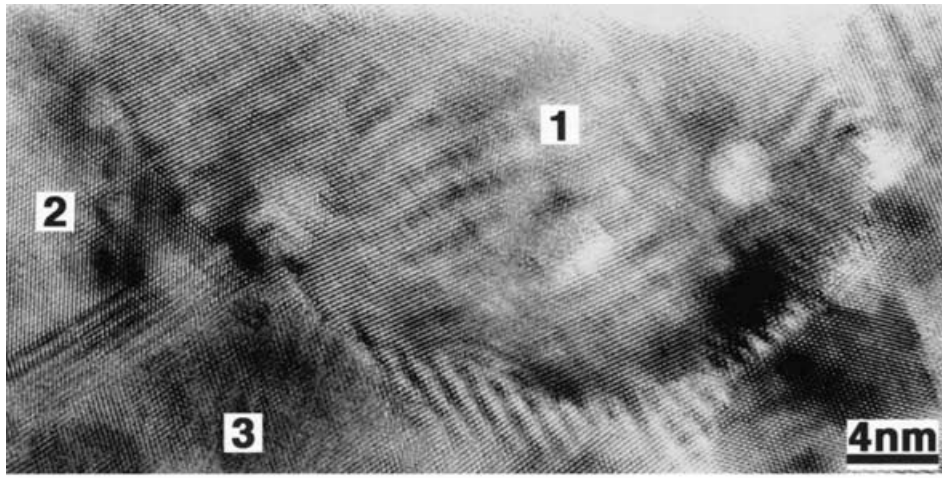

Figure 8. GBs among three grains.

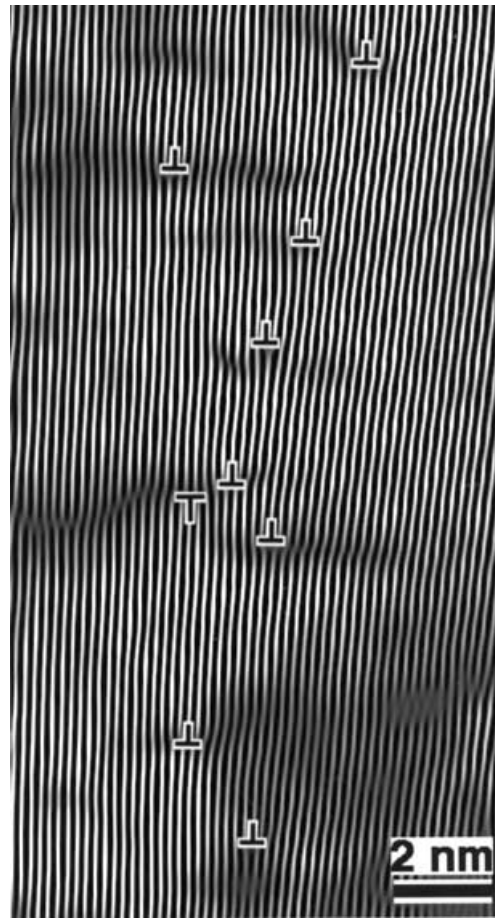

Figure 9. A near-symmetrical SAGB. The T and inverted Ts indicate the cores of the GB dislocations.

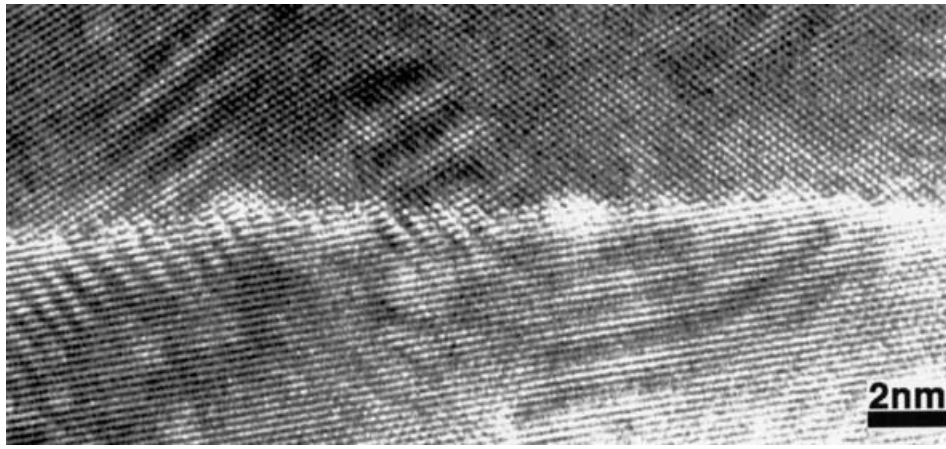

Figure 10. A near $\Sigma = 11$ GB. The GB plane is straight and slightly strained.

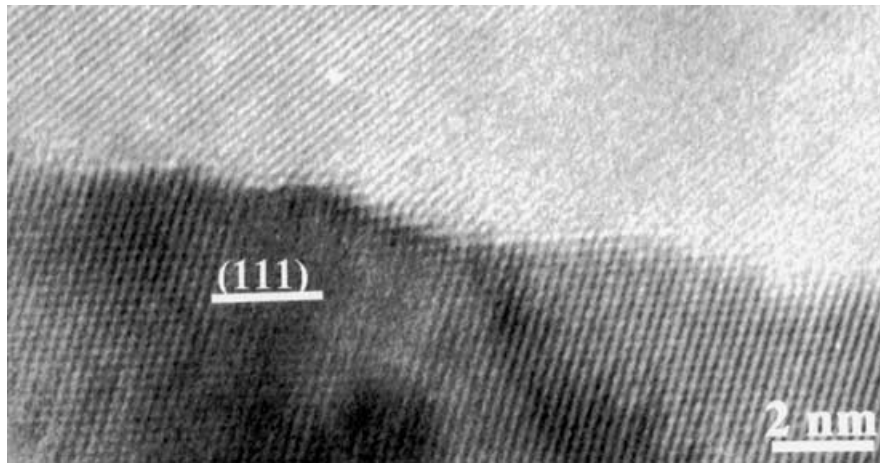

Figure 11. A GB containing facets on (111) planes and steps.

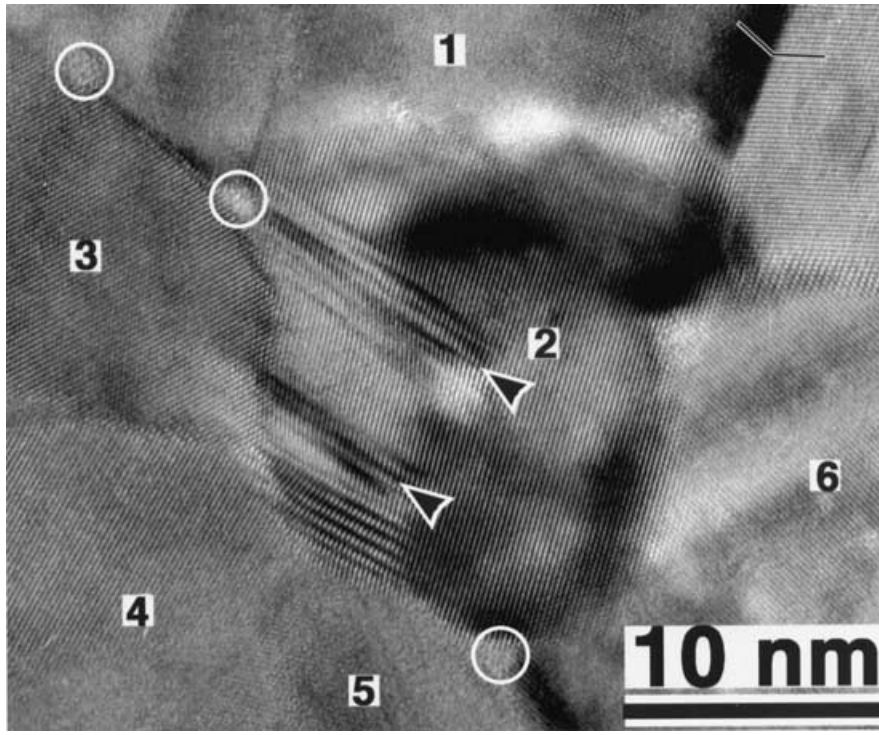

Figure 12. Nanograins and GBs in cryomilled Cu. The arrowheads indicate SFs or thin twins. Note that SFs or thin twins initiated from the GB and terminated in the interior of grain 2. The white circles outline disordered regions in the GBs. The white-edge black lines in the upper right corner indicate a twin. The numbers 1–6 indicate grains.

§ 4. Discussion

4.1. *Grain refinement mechanism during ball milling*

The process of grain refinement during large strain deformation has been discussed by Hughes and Hansen (1997), Hughes *et al*. (1997) and Zhu and Lowe (2000). With increasing strain, cell blocks separated by geometrically necessary boundaries form within grains and cellular structures with incidental dislocation boundaries form within grains. The misorientations of geometrically necessary boundaries and incidental dislocation boundaries increase with increasing strain, and some of these boundaries may become LAGBs with sufficient strain. Ball milling is a large strain deformation process. The present HREM results indicate that the grain refinement mechanism in the ball-milling process is similar to that proposed above. In short, it suggests that grain refinement during ball milling is a continuous process that consists of formation of dislocation subboundaries, such as SAGBs in this case, a gradual rise in the SAGB misorientation due to accumulation of more dislocations and, finally, the formation of LAGB.

4.2. *Non-equilibrium grain boundary*

The microstructures developed by cold or high-strain deformation are characterized by a relatively high density of dislocation substructures and, therefore, a high stored energy. Such strain-induced GBs can be in a non-equilibrium state (Horita *et al*. 1996, 1998, Huang *et al*. 2001, Valiev *et al*. 2000). Non-equilibrium GBs can lead to changes in fundamental physical and mechanical properties, such as the elastic moduli, diffusion coefficient, strength, superplasticity and magnetic properties of nanostructured materials. Extrinsic dislocations, which are not geometrically necessary, are frequently observed in cryomilled Cu (such as that shown in figure 7), indicating that the GBs are mostly in non-equilibrium configurations. Similar non-equilibrium GBs were also found in RCS-processed Cu (Huang *et al*. 2001) and in ECAP-processed Al–Mg (Horita *et al*. 1996), indicating that non-equilibrium GBs can exist in nanostructured metals produced by different deformation methods. It should be mentioned that the grain size obtained by ball milling is usually much smaller than that produced by ECAP or RCS. In the former case, the grain size is normally less than 100 nm while, in the latter two cases, it is around 500 nm.

§ 5. Conclusions

(1) The grain refinement during ball milling is a strain-induced continuous process that consists of formation of dislocation subboundaries, such as SAGB, a gradual increase in the subboundary misorientation due to accumulation of more dislocations and, finally, the formation of a LAGB.
(2) The GBs of cryomilled Cu are generally curved, or wavy with non-uniform contrast, or faceted, which are general features in nanostructured materials.
(3) The GBs in cryomilled Cu are in a high-energy non-equilibrium configurations. The similarity between the cryomilled Cu, room-temperature ball-milled Cu, ECAP-processed Cu and RCS-processed Cu suggests that non-equilibrium GBs are typical features of nanostructured metals and alloys processed using severe plastic deformation techniques.

Acknowledgements

We thank Dr D. W. He for performing the cold compaction of the milled powders. F. Z. and E. J. L. acknowledge the financial support from the Office of Naval Research under grants N00014-00-1-0109 and N00014-01-1-0882 with Dr Lawrence Kabacoff as program officer.

References

Horita, Z., Smith, D. J., Furukawa, M., Nemoto, M., Valiev, R. Z., and Langdon, T. G., 1996, *J. Mater. Res.,* **11**, 1880.

Horita, Z., Smith, D. J., Nemoto, M., Valiev, R. Z., and Langdon, T. G., 1998, *J. Mater. Res.,* **13**, 446.

Huang, J. Y., 1999, *Acta mater.,* **47**, 1801.

Huang, J. Y., He, A. Q., Wu, Y. K., and Ye, H. Q., 1994a, *J. Mater. Sci. Lett.,* **13**, 1201.

Huang, J. Y., Jiang, J. Z., Yasuda, H., and Mori, H., 1998a, *Phys. Rev.* B, **58**, R11817.

Huang, J. Y., Wu, Y. K., and Ye, H. Q., 1994b, *Mater. Lett.,* **21**, 167; 1996, *Acta mater.,* **44**, 1211; 1998b, *Microsc. Res. Tech.,* **40**, 101.

Huang, J. Y., Yu, Y. D., Wu., Y. K., Li, D. X., and Ye, H. Q., 1997a, *J. Mater. Res.,* **2**, 936.

Huang, J. Y., Yu, Y. D., Wu, Y. K., and Ye, H. Q., 1997b, *Acta mater.,* **45**, 113.

Huang, J. Y., Zhu, Y. T., Jiang, H., and Lowe, T. C., 2001, *Acta mater.,* **49**, 1497.

Hughes, D. A., and Hansen, N., 1997, *Acta mater.,* **45**, 3871.

Hughes, D. A., Liu, Q., Chrzan, D. C., and Hansen, N., 1997, *Acta mater.,* **45**, 105.

Liao, X. Z., Huang, J. Y., Zhu, Y. T., Zhou, F., and Lavernia, E. J., 2002 (submitted).

Shen, T. D., Koch, C. C., McCormic, T. L., Nemanich, R. L., Huang, J. Y., and Huang, J. G., 1996, *J. Mater. Res.,* **10**, 139.

Valiev, R. Z., Islamgaliev, R. K., and Alexandrou, I. V., 2000, *Prog. Mater. Sci.,* **45**, 103.

Yang, X. Y., Shi, G. Y., Meng, X. M., Huang, H. L., and Wu, Y. K., 1999, *Acta crystallogr.* B, **55**, 255.

Yang, X., Wu, Y. K., and Ye, H. Q., 2000, *Phil. Mag. Lett.,* **80**, 333.

Zhu, T., and Lowe, T. C., 2002, *Mater. Sci. Engng,* **A291**, 46.